Nano Energy 93 (2022) 106884

Contents lists available at ScienceDirect

Nano Energy

journal homepage: www.elsevier.com/locate/nanoen

Methods for correctly characterizing the output performance of nanogenerators☆

Jie An [a,b,1], Pengfei Chen [a,b,1], Chengyu Li [a,b], Fangming Li [d], Tao Jiang [a,b,c,*], Zhong Lin Wang [a,b,c,e,**]

[a] Beijing Institute of Nanoenergy and Nanosystems, Chinese Academy of Sciences, Beijing 101400, China
[b] School of Nanoscience and Technology, University of Chinese Academy of Sciences, Beijing 100049, China
[c] CUSTech Institute of Technology, Wenzhou, Zhejiang 325024, China
[d] Marine Engineering College, Dalian Maritime University, Dalian 116026, China
[e] School of Materials Science and Engineering, Georgia Institute of Technology, Atlanta, GA 30332-0245, USA

ARTICLE INFO

Keywords:
Characterization methods
Output performance characterization
Multi-functional electrometer
Nanogenerator
Voltage measurement error
Multiphysics simulation

ABSTRACT

Nanogenerators (NGs) based on triboelectric effect, piezoelectric effect, and pyroelectric effect have rapidly developed in applications of energy harvesting and self-powered sensing. However, a standard output performance characterization system for NG devices is still lacking, which greatly reduces the reference and inheritance of scientific research results, and hinders the development of NG technology. Owing to the mismatch of impedance between the instrument and NG devices, commercial instruments have serious measurement error of up to 77.3%, which causes some experimental phenomena violating the theories. In this work, the influencing factors of measurement error from traditional measurement methods are systematically analyzed through Multiphysics simulations and comparison experiments. Some methods to improve the accuracy are proposed, and a multi-functional and high-precision instrument is designed to improve the measurement accuracy from 22.7% to 64.7%. This discovery points out the shortcomings of the current characterization methods of NG performance, which has important guiding meaning for the development of measurement technology and theoretical research of NGs.

1. Introduction

The development of internet of things requires various distributed electronic devices [1,2]. The difficulty of uninterrupted power supply for these huge-number, widely-distributed, and mobile electronic devices has caused widespread concerns [3]. Combining new technologies to decrease energy consumption and harvest energy from surrounding environment is a feasible solution [4–10]. Nanogenerators (NGs) including triboelectric nanogenerator (TENG) [11], piezoelectric nanogenerator (PENG) [12,13], and pyroelectric nanogenerator [14], etc. [15], have been developed as new technologies for weak energy harvesting and self-powered sensing. Owing to the advantages of excellent output performance in low frequency, wide material selection, easy fabrication, and low cost, the development of TENG research is particularly rapid [16–26]. Many works based on TENG about energy harvesting and self-powered sensors have been reported, such as wind energy [27,28], blue energy [29–33], rain drop energy [34], and vibration energy [35] harvesting, as well as self-powered angle sensors [36], touch sensors [5,37], and liquid level sensors [6], etc. [8,38–40].

Essentially speaking, the NGs use displacement current as the driving force for effectively converting mechanical energy into electric power/signal [41]. Therefore, these kinds of charge-based devices can be equivalent to a lumped model with a voltage source and a capacitor in series [42,43]. The reciprocating transfer of the charges with limited

☆ Prof Zhong Lin Wang, a corresponding author on this paper, is the Editor-in-Chief of Nano Energy, but he had no involvement in the peer review process used to assess this work submitted to Nano Energy. This paper was assessed and the corresponding peer review managed by Professor Chenguo Hu, also an Associate Editor in Nano Energy.

* Corresponding author at: Beijing Institute of Nanoenergy and Nanosystems, Chinese Academy of Sciences, Beijing 101400, China.
** Corresponding author at: School of Materials Science and Engineering, Georgia Institute of Technology, Atlanta, GA 30332-0245, USA.
E-mail addresses: jiangtao@binn.cas.cn (T. Jiang), zlwang@gatech.edu (Z.L. Wang).
[1] These authors contributed equally to this work.

https://doi.org/10.1016/j.nanoen.2021.106884
Received 17 November 2021; Received in revised form 12 December 2021; Accepted 24 December 2021
Available online 29 December 2021

amount in the external circuit drives the electronic components to work. Traditional voltage measurement method based on resistor divider will lead to the loss of charges through the resistor [42]. The loss of charges will cause a large distortion in the voltage measurement at low-frequency motion of NGs. The problems existing in traditional measurement methods make it difficult to correctly measure the signals of NGs [44], which also hinders its development in self-powered sensing technology. Electrometers can measure the amount and direction of charge transfer, and the voltage of the device can be derived by measuring the amount of the charges flowing through the internal capacitor of instrument, which is not affected by the moving frequency of the devices. However, if the internal capacitance of the electrometer is too large, too many charges will flow through the measurement circuit resulting in the voltage decrease of NGs. At present, the characterization of nanogenerators generally uses a commercial 6514 electrometer. Its internal capacitance is 300 pF, which is close to or larger than the equivalent capacitance of most NGs. Such a large internal capacitance of the instrument will inevitably affect the signal source and cause measurement errors [45]. The V-Q cycle curve can effectively reflect the output performance of NG. If the voltage measurement error is too large, the area of measured energy output cycles will be much lower than the theoretical result, which will mislead the development of theory and the determination of experimental conclusions. Due to the limitations of measuring instruments, the characterization of NGs has never formed a unified standard. The varied measurement results using different instruments will greatly reduce the reference and inheritance of scientific research results, and hinder the development of nanogenerator technology.

In this work, the influence of measuring instruments on experimental results is explored to improve the characterization accuracy. By systematically studying the influences of instrument capacitance and TENG equivalent capacitance on the measured voltage, the influence rule is obtained, and the inner principle is revealed. An ideal NG is constructed using a known voltage source and a capacitor in series to accurately characterize the measurement error of instrument, and the reason that many experimental results deviate from the Kirchhoff voltage law is also explained by this measurement error. Combined with Multiphysics simulations for four working modes of TENGs, an optimization strategy of instrument parameters is established. Finally, we design a modified multi-functional instrument for the output performance characterization of NGs, and the measurement error is significantly decreased compared to the commercial 6514 electrometer. The proposed measurement error and optimization strategy have great significance for constructing a standard characterization system for NGs, which is beneficial for the development of measurement technologies and theoretical researches of NGs, as well as their applications in self-powered

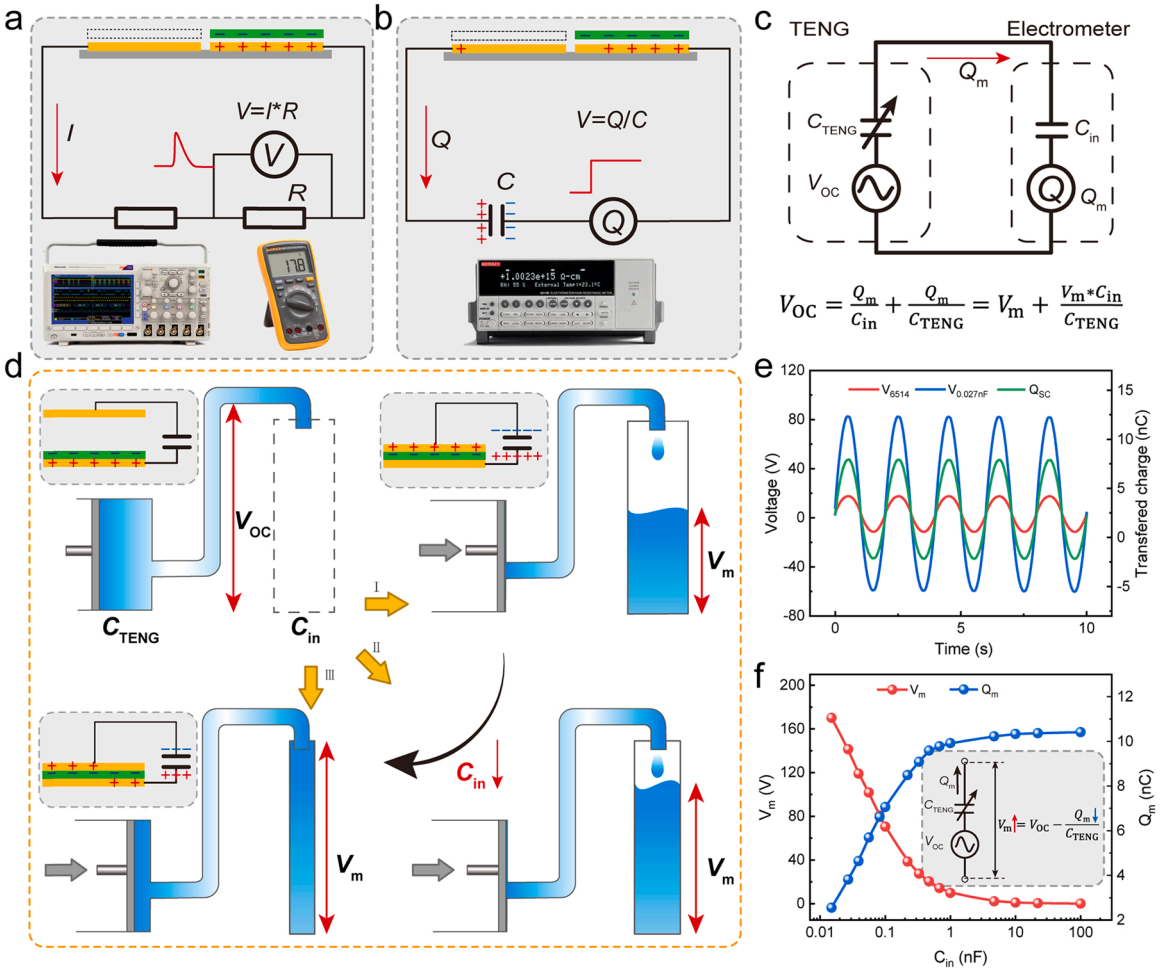

Fig. 1. Demonstration of the reason why the measurement method and internal impedance of voltmeter seriously affect the voltage measurement results of charge-based devices. (a–b) Principles of measuring the output voltage of TENG with (a) resistance-based and (b) capacitance-based instruments, respectively. (c) Equivalent circuit of an electrometer measuring the output voltage of TENG and the relationship between V_m/V_{OC} and C_{in}/C_{TENG}. (d) Schematic illustration for the influence of the instrument internal capacitance on the measured voltage. (e) Waveform comparison of measured voltage and short-circuit transferred charge measured by a 6514 electrometer and a modified electrometer with the C_{in} of 0.027 nF. (f) Variation of measured voltage and transferred charge with the increase of C_{in}. The insert illustrates their theoretical relationship.

sensing technology.

2. Results and discussion

2.1. Influencing principle of instrument impedance on the measurement results

A sliding freestanding triboelectric-layer (SFT) mode TENG is taken as an example to show and explain the measurement methods of NGs. According to the difference of measurement principle, it can be divided into two kinds of voltage measurement methods. One method is to obtain the voltage of the TENG indirectly by measuring the voltage of divider resistor, as illustrated in Fig. 1**a**. This method has been universally utilized in oscilloscope, multimeter, and data acquisition card as a general technology. Owing to the limited charge amount of TENGs, the induced charges in the copper will flow through the resistor as the dielectric layer slides rightward. The measured waveform of voltage is as same as the current in the circuit according to the equation of $V = I * R$, which is related to the charge transfer speed, so the measured signal is severely distorted under low working frequency of TENG. The other method is to derive the voltage from the relation of $V = Q/C$ by measuring the amount of charges flowing through the capacitor, as illustrated in Fig. 1**b**. High waveform fidelity can be maintained in the process of measuring voltage signals of TENG, even at low working frequency, due to the similar impedance between TENG and instrument. However, if the capacitance of instrument does not match with the equivalent capacitance of TENG, the measured value of voltage V_m will be far away from the actual open-circuit voltage V_{OC}.

The relationship between V_{OC} and V_m is shown as the equation in Fig. 1**c.** When the ratio of C_{in}/C_{TENG} trends to zero, the measured voltage will gradually get close to the actual V_{OC}. The underlying principle can be explained visually by Fig. 1**d.** Because of the similarity between the charge and liquid, the nanogenerator can be equivalent to a pump with the capacity of C_{TENG} and hydraulic head of V_{OC}. Similarly, the internal capacitor of instrument can be considered as a container, whose capacity is related to the capacitance C_{in}. When the capacitance of instrument is large, the measured voltage V_m is limited by the inherent capacity of C_{TENG} even though the V_{OC} is high. As the capacitance C_{in} decreases from state I to III, the measured voltage will gradually increase until it approaches the V_{OC}. From above illustration, we can intuitively understand the influence of the instrument capacitance on the measured voltage. When the C_{in} is decreased to 0.027 nF, the measured voltage is significantly increased from 30 V to 140 V compared to that from the 6514 electrometer (C_{in} = 0.3 nF) for a practical SFT mode TENG, as shown in Fig. 1**e and** Supplementary Fig. 1. The comparison demonstrates that the capacitance C_{in} only affects the amplitude value of measured voltage, but the waveform will remain consistent. The amplitude variation trends of V_m and transferred charge Q_m in the circuit with respect to the C_{in} are shown in Fig. 1**f.** The decrease of C_{in} will block the charge transfer in the circuit, leading to lower partial voltage of C_{TENG} and higher measured voltage (see the inset). Therefore, it can be concluded that the internal capacitance of instrument should be as small as possible to reduce the interference to the signals when measuring the open-circuit voltage of TENGs. The other method to overcome the measurement problem from the limited charge of NG is shown in Supplementary Fig. 2.

2.2. Characterization of the relationship between the capacitance and measurement error

We have realized that the capacitances C_{in} and C_{TENG} will affect the measured voltage, but the measurement error between V_m and V_{OC} deserves to be further studied. Since there is no instruments that can accurately measure the V_{OC} of NGs, an ideal NG is constructed with a given voltage source (amplitude: 20 V/10 V) and a capacitance (100 pF) to analyze the measurement error, as illustrated in Fig. 2**a**. The 6514 electrometer can be equivalent to a capacitor of 300 pF connected with a coulombmeter in series. According to the relationship of $V_m = \frac{Q_m}{C_{in}}$, the electrometer can acquire the V_m by measuring the transferred charge amount through the instrument. When the capacitance C_{TENG} increases, the measured voltage by the 6514 electrometer increases accordingly and approaches gradually the V_{OC} (Fig. 2**b**). It means that larger equivalent capacitance of NG is beneficial for the improvement of voltage measurement accuracy. In the experiments, different kinds of voltage source waveforms are applied to simulate different motion modes of TENG, such as sinusoid wave, square wave, and sawtooth wave.

The measured voltage is linearly related to the V_{OC} for different C_{TENG}, and it is independent of the voltage source waveform (Fig. 2**c and** Supplementary Fig. 3), which means the V_m have the same waveform as the V_{OC}, and the capacitance C_{TENG} only influences the amplitude of V_m. The slopes of V_m-V_{OC} curves can be found to gradually trend to 1 with the increase of C_{TENG}, as shown in Fig. 2**d**. According to the equation

$$M_{Error} = \frac{V_{OC} - V_m}{V_{OC}} = 1 - \frac{V_m}{V_{OC}} \tag{1}$$

the measurement error M_{Error} is also decreased accordingly with increasing the C_{TENG}. The internal equivalent capacitance of the 6514 electrometer can be deduced to be about 350 pF (Fig. 2**e)** by the equation

$$C_{6514} = \left(\frac{V_{OC}}{V_m} - 1\right) * C_{TENG} \tag{2}$$

which is comparable with the nominal value of 300 pF. For an actual NG, the equivalent capacitance C_{TENG} is usually less than 1 nF, therefore, the measurement error may be very high when directly measuring the voltage by the 6514 electrometer. One modified method is to measure the short-circuit transferred charge of the NG (Fig. 2**f)** and calculate the V_{OC} by

$$V_{OC} = \frac{Q_{SC}}{C_{TENG}} \tag{3}$$

Owing to the constant capacitance of C_{TENG} used in this ideal NG, the measured Q_{SC} is linearly related to the V_{OC} (Fig. 2**g and** Supplementary Fig. 4), and the amplitude of calculated V_{OC} is very close to the actual value of 20 V for different C_{TENG} applied (Fig. 2**h**). However, the capacitance C_{TENG} usually varies simultaneously with the V_{OC} for an actual NG, bringing a difficulty to obtain the V_{OC} through Eq. (3). A possible solution is to introduce a constant sampling capacitor C_s like the internal capacitor of 6514 electrometer in voltage mode, as shown in Fig. 2**i**, but its capacitance needs to be modified. The transferred charge in the circuit is decreased for smaller capacitance C_s, which is beneficial for improving the measurement accuracy because of the decrease of Q_m **(**Fig. 2**j)**. When the C_s is decreased to 0.027 nF, the measured voltage is increased to 17.5 V **(**Fig. 2**k)**, with a measurement error of 12.5% according to Eq. (1)**.** When the internal capacitance of instrument is 100 times smaller than NG equivalent capacitance, the open-circuit voltage is almost shared by the instrument, and the measured voltage can be considered as the open-circuit voltage.

2.3. Phenomenon that the experimental results do not conform to the theoretical laws caused by the measurement error

Series and parallel connections between electronic components are usually used to achieve higher voltage or current. When two ordinary voltage sources are connected in series, their output voltage will be superimposed. However, when multiple TENGs are connected in series or parallel as illustrated in Fig. 3**a,** the parallel voltage is significantly higher than the series voltage measured by the 6514 electrometer (Fig. 3**b**), which is far away from the Kirchhoff's voltage law. In order to understand the reason, we need to analyze how to measure the open-

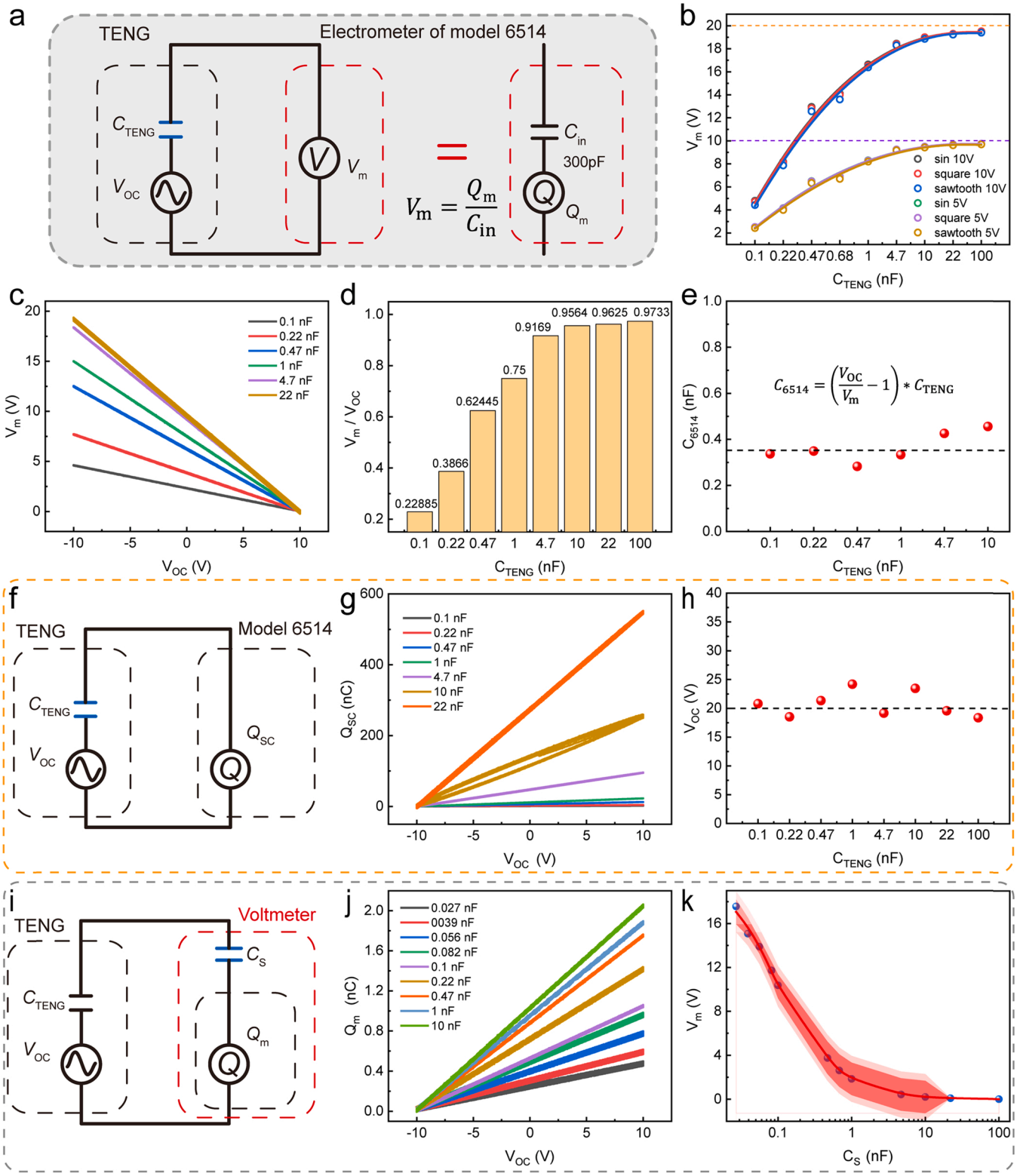

Fig. 2. Systematical and quantitative characterization for the influences of C_{TENG} and C_{in} on the measured voltage. (a) Schematic circuit utilized in the next characterization. A voltage source and a capacitance are connected in series to form an ideal TENG. (b) Variation of the measured peak voltage using a 6514 electrometer with the increase of C_{TENG} for different waveforms and amplitudes of voltage source. (c) The linear relationship and (d) the slope between the V_m and V_{OC} for different C_{TENG}. (e) Derived C_{in} of the 6514 electrometer at different C_{TENG} according to the inserted theoretical equation. (f) Schematic circuit for measuring the V_{OC} of TENG according to the Q_{SC} and C_{TENG}. (g) The linear relationship between the Q_{SC} and V_{OC} for different C_{TENG}. (h) Derived peak values of V_{OC} according to the relationship of $V_{OC} = Q_{SC}/C_{TENG}$, which are close to the actual value for different C_{TENG} applied. (i) Schematic circuit for measuring the V_{OC} of TENG by introducing a sampling capacitance C_s. (j) The linear relationship between Q_m and V_{OC} for different C_s applied at a fixed C_{TENG} of 0.1 nF. (k) Variation of measured voltage with the C_s. The V_m gradually approaches the V_{OC} of 20 V with the decrease of C_s.

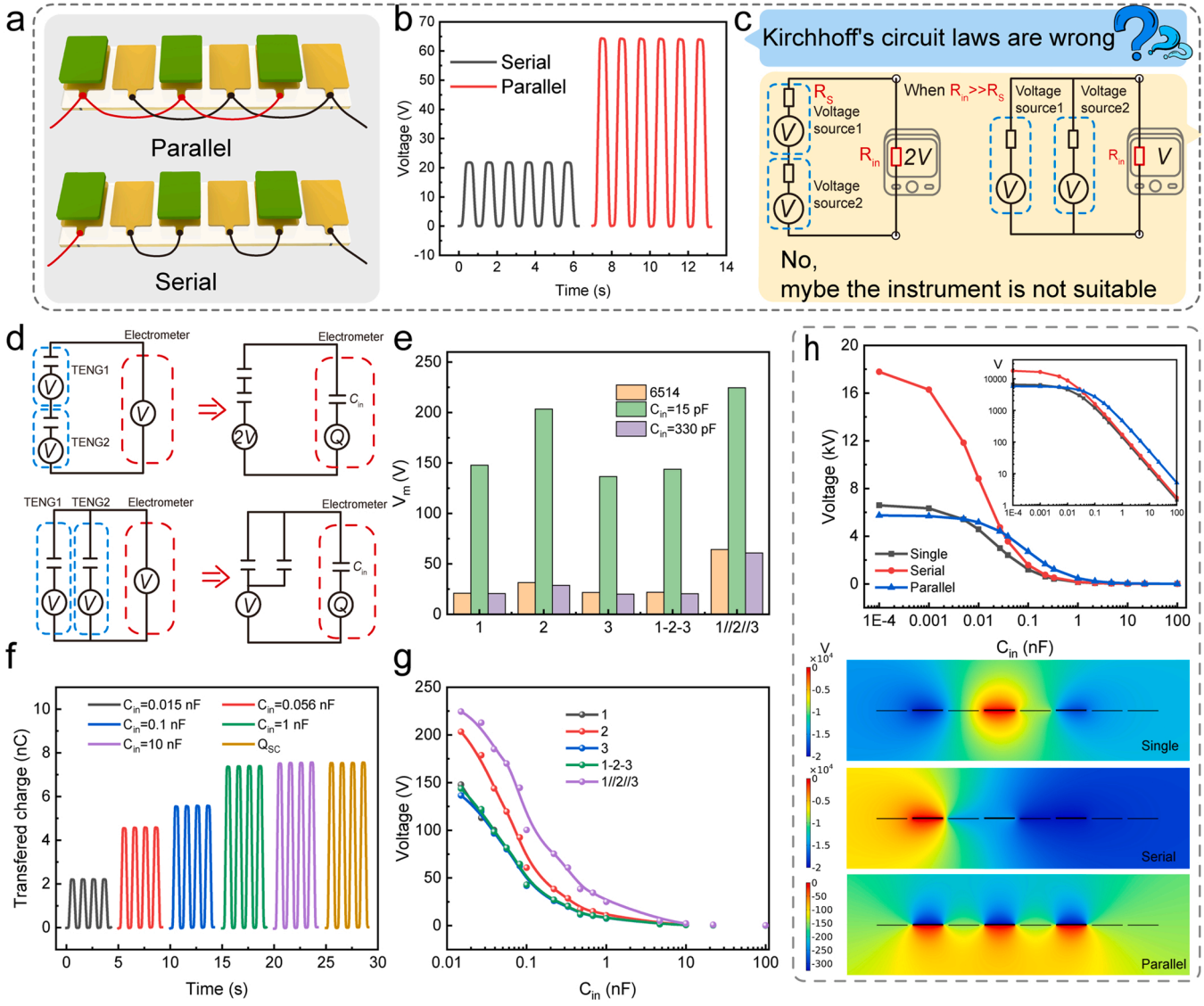

Fig. 3. Demonstration of the reason why the series and parallel voltages of TENG measured by a 6514 electrometer do not accord with the Kirchhoff's voltage law. (a) The illustration and (b) the voltage waveform of the parallel and series connection of three groups of TENGs measured by the 6514 electrometer. (c) Presentation of the question that the measurement result does not follow the Kirchhoff's voltage law, and explanation of the potential reason by analogy with traditional measurement methods. (d) Equivalent circuits of series and parallel connections of two TENGs, respectively. (e) Comparison of three TENGs' voltage and their series and parallel voltages measured by different instruments with different internal capacitances. The voltage amplitudes measured by the 6514 electrometer and an electrometer with the C_{in} of 330 pF are very close, due to the proximity of their internal capacitance. (f) Waveform variation of Q_m with the increase of C_{in}. The amplitude trend of measured voltage (g) and simulated voltage (h) with the decrease of C_{in} for TENG1, 2, 3, and their series and parallel connections. The inset of Fig. 3h shows the diagram with log ordinate, and the bottom shows the typical potential distributions at $C_{in} = 0.1$ pF.

circuit voltage of an ordinary power source. As illustrated in Fig. 3**c,** the essential condition for the measurement of the open-circuit voltage is the much larger impedance of instrument than internal impedance of voltage source. Under this condition, the current in the circuit is minimized and the divided voltage by internal resistance of power source can be ignored, so the measurement results will accord with the serial and parallel correlation theory for an ordinary power source. The measurement of NGs also has similar restrictions to minimize the transferred charge in the circuit and improve the measurement accuracy.

The equivalent circuits of two TENGs connected in series and parallel are illustrated in Fig. 3**d**. The open-circuit voltage is doubled for two TENGs in series, but the equivalent capacitance of TENG is halved, which will further increase the measurement error and decrease the V_m. By contrast, the open-circuit voltage does not change for the parallel connection, but the equivalent capacitance of TENG is doubled, which will decrease the measurement error and increase the V_m. Eventually, the parallel voltage is higher than the series voltage even though the instrument capacitance is decreased to 15 pF (Fig. 3**e**), because the transferred charge at $C_{in} = 15$ pF is not small enough (Fig. 3**f**). The variations of measured voltage for three TENGs as well as their serial and parallel connections are shown in Fig. 3**g**. With the decrease of C_{in}, the parallel voltage is gradually reaching saturation but the series voltage continuously rises rapidly, implying that the capacitance needs to be further decreased to accurately measure the voltage. Because it's difficult to measure the very small transferred charge amount by a commercial instrument at smaller C_{in}, a Multiphysics simulation model is built to obtain the voltage at smaller C_{in}, as shown in Fig. 3**h**. It can be seen that the parallel voltage is equal to the voltage of a single TENG, while the series voltage is the sum of three TENGs' voltages when the C_{in} is decreased to 0.1 pF, which conforms to the Kirchhoff's voltage law. The above experiments prove that the experimental error is the main reason for the discrepancy between many experimental phenomena and

theories, and demonstrate that the improvement of measurement accuracy is of great significance to the mutual guidance of experimental and theoretical researches for NGs.

2.4. Multiphysics simulation analysis for four working modes of TENGs

In order to systematically compare the influence of instrument capacitance on the output voltage of four working modes of TENGs, a standard simulation model is constructed by coupling electrostatic field, circuit, and moving mesh technology. The boundary conditions and physics settings for the simulations of contact-separation (CS) mode TENG are shown in Fig. 4**a**. In the previous simulation works about TENG, the steady-state potential distribution around the charged body was mainly investigated, but the dynamic behaviors of TENGs under external triggering when connecting with an external resistive or capacitive load were rarely considered [46]. Benefiting from Multiphysics fully-coupled simulations, the model can obtain the time-varying electric outputs when a sinusoidal motion is applied to the TENG. The simulated voltage output is very consistent with the experimental result at an external load of 1 GΩ, as illustrated in Fig. 4**b**, which demonstrates the authenticity and advancement of the simulation method. When a capacitor is connected to the CS mode TENG in parallel to simulate the measurement process of the instrument, a significant decrease of voltage amplitude is caused by the larger C_{in}, as presented in Fig. 4**c**.

Supplementary material related to this article can be found online at

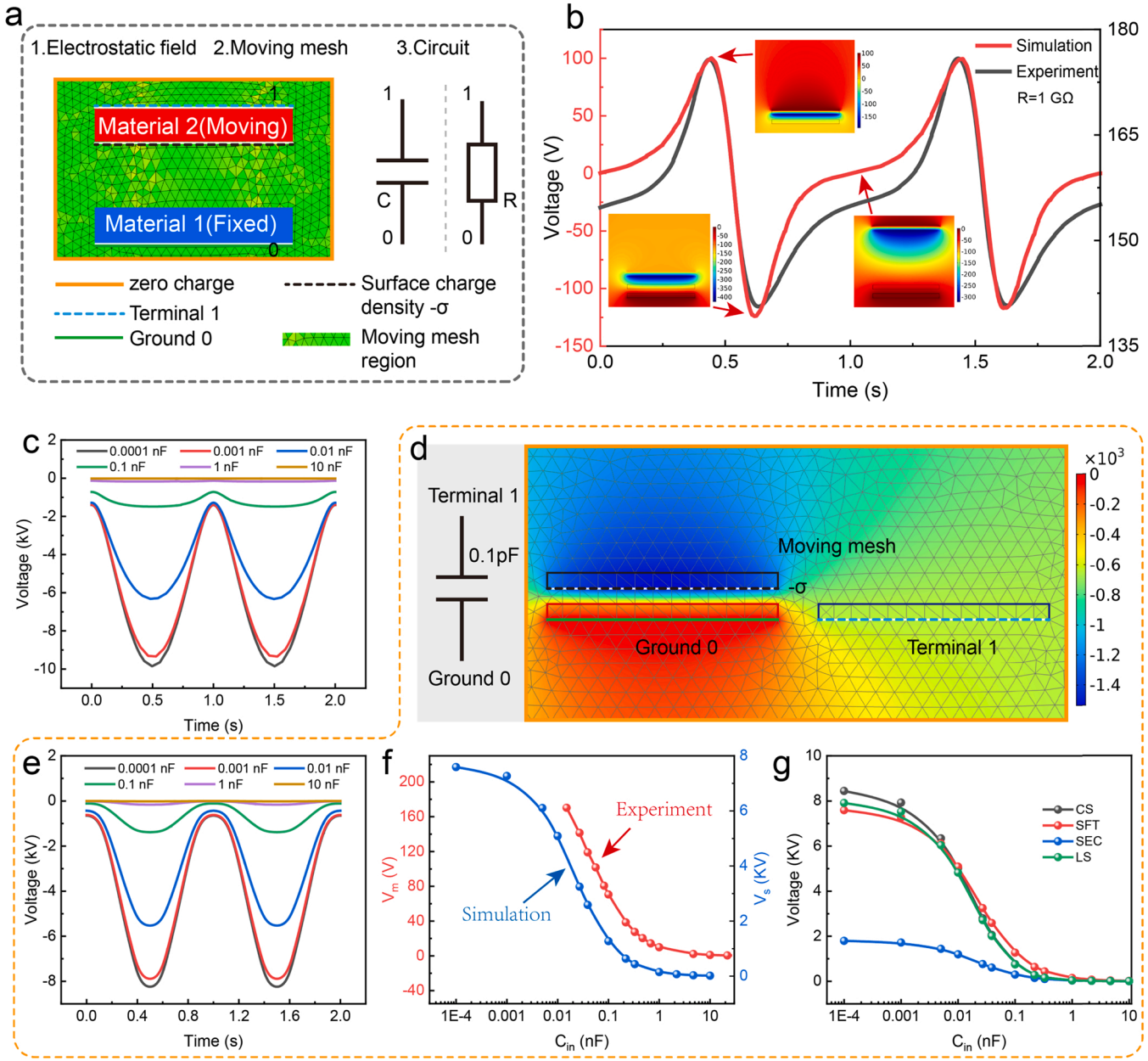

Fig. 4. Simulation analysis of the influence of instrument C_{in} on the measurement results for four modes of TENGs through a standard Multiphysics simulation method. (a) Physics and boundary condition settings for the CS mode TENG. (b) Simulated dynamic output voltage and electric potential distribution of TENG when loading a resistor of 1 GΩ. (c) Simulated dynamic output voltage of CS-TENG under different capacitive loads. (d) Physics and boundary condition settings for the SFT mode TENG. (e) Simulated dynamic output voltage of the SFT-TENG under different capacitive loads. (f) Comparison diagram between the simulation and experimental results for the voltage amplitude versus the capacitance. (g) Variation curves of voltage amplitude with respect to the loaded capacitance for four modes of TENGs.

doi:10.1016/j.nanoen.2021.106884.

Subsequently, an SFT mode TENG model is also constructed for comparison, which has the same charge density σ and electrode area (Fig. 4**d**). The capacitance C_{in} has the similar effect on the voltage amplitude as the CS mode TENG (Fig. 4**e and** Supplementary Fig. 5), but its voltage waveform is more symmetrical due to the structural symmetry of SFT mode TENG. By comparing the simulation results with the experiments, it can be found that two profiles of voltage amplitude versus the capacitance C_{in} can be well matched, which further confirms the accuracy of the simulation method (Fig. 4**f**). It should be noted that

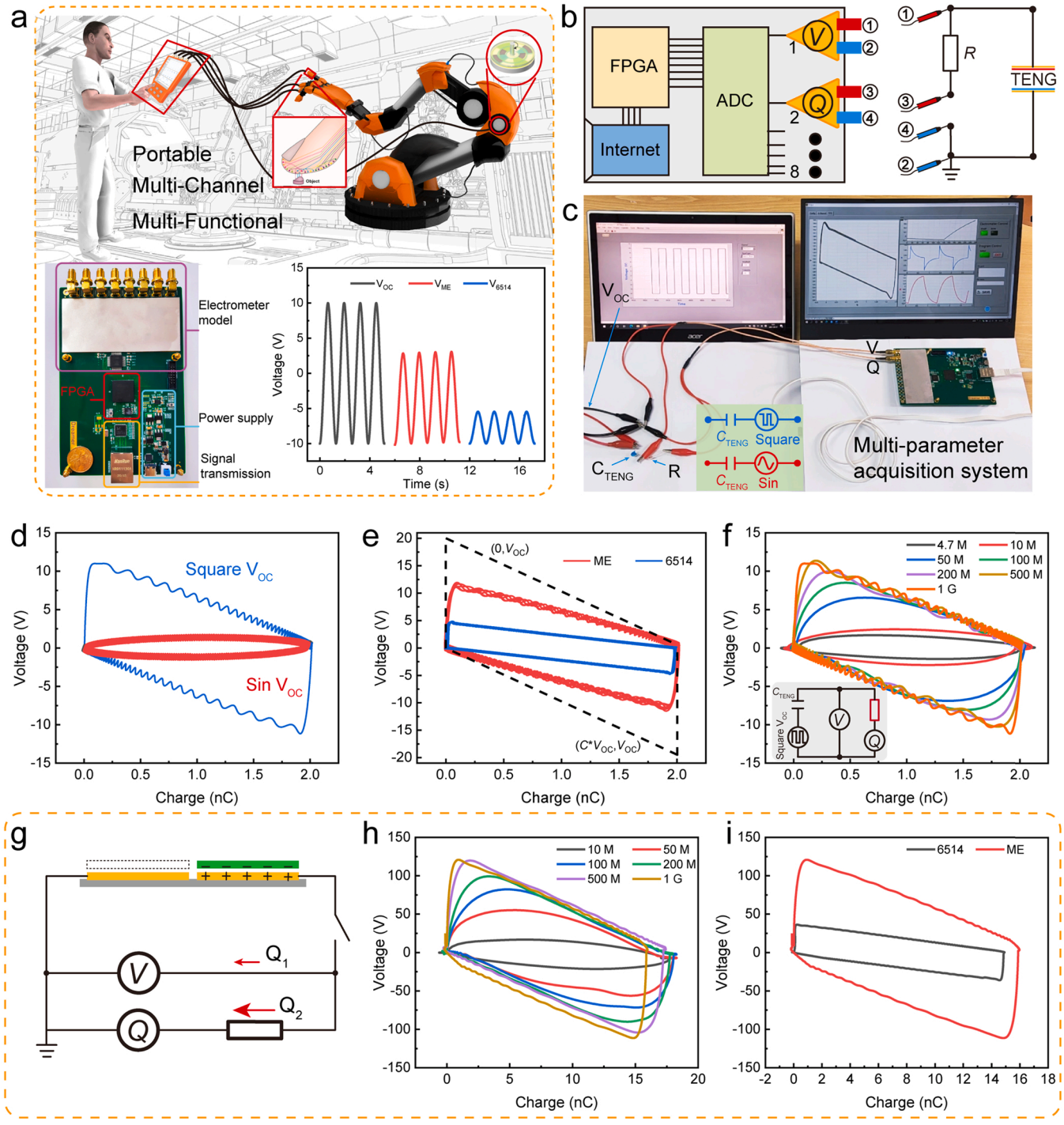

Fig. 5. Energy output cycle characterization of NGs using the optimized characterization system. (a) Application concept of a NG testing system with merits of portability, multi-channel, and multi-function to realize the field testing of various parameters of the NG devices. The bottom shows the photograph of the multi-channel electrometer and voltage comparison measured by the 6514 electrometer and ME with the V_{OC}. (b) Schematic diagram of acquiring *V-Q* profile of TENG by the ME. (c) The photograph of *V-Q* curve acquisition system for characterizing two different modes of ideal NG. The normal and MEC working modes of TENG are simulated using different voltage sources, and (d) their comparison of energy output cycles measured by the ME. (e) The comparison of the MEC measured by the ME and 6514 electrometer with the theoretical maximum cycle. (f) Energy output cycles of ideal TENG under different external loads. (g) Circuit diagram of energy output cycle characterization for practical SFT-TENG. (h) Energy output cycle curves of the SFT mode TENG under different external loads. (i) Comparison for the MEC of the SFT mode TENG obtained by the 6514 electrometer and ME.

the difference between the experimental measured value and simulation value is caused by the deviation of the set value of charge density from the reality. When the C_{in} is reduced to 15 pF, the tiny transferred charge in the circuit is difficult to be measured, hindering the voltage measurement by the instrument, but this problem can be overcome through simulations, and the trend of V_m can be obtained at smaller C_{in}. Finally, the other two modes of TENGs are also simulated and analyzed (Supplementary Fig. 6 **and** Supplementary Movie 1**),** and the variation curves for the voltage amplitude of four modes of TENGs are summarized in Fig. 4**g.** With the decrease of paralleled capacitance, the voltage amplitude gradually approaches the open-circuit voltage for four modes of TENGs, because of the voltage decrease shared by the C_{TENG}. The voltage of single-electrode contact (SEC) mode TENG is markedly lower than that of others due to its smaller equivalent capacitance. In order to accurately measure the voltage of the four modes TENGs, the instrument capacitance needs to be less than 1 pF for the SEC mode TENG and 0.1 pF for other modes. The simulation analysis overcomes the shortcomings of the experiments, which makes it possible to compare the signal difference for different modes of TENGs while maintaining the same electrode area and charge amount on the dielectric layer. At the same time, it makes possibility of obtaining the complete V_m trend with the C_{in}, and the suitable internal capacitance of instrument to achieve the measured results close to the V_{OC}.

2.5. Modified multi-functional characterization system of NGs

With the rapid development of NG technology, it's urgent to construct a standard characterization system and special measurement instrument with merits of portability, multi-channel, and multi-function to meet the requirements of outdoor and field testing. After the optimization many times, a modified electrometer (ME) with eight channels is designed as shown in Fig. 5**a.** After calibration, the electrometer can accurately measure conventional voltage signals, and the measurement error is decreased from 77.3% to 35.3% compared to the commercial 6514 electrometer for a NG with $V_{OC} = 20$ V, and $C_{TENG} = 100$ pF (bottom of Fig. 5**a and** Supplementary Fig. 7). Not only the ME can realize synchronous signal acquisition of multiple sensors, but also each channel can be configured as voltage, current, or charge gauge to synchronously acquire the *V-Q* curve to characterize the output performance of a NG [47]. The system composition of the ME and the measurement circuit of *V-Q* curves are shown in Fig. 5**b.** Channel 1 is configured to measure the voltage on the external load *R*, and channel 2 is configured to measure the transferred charge through the circuit. The analog signals from these two channels are acquired and converted to digital signals, and then sent to a computer for real-time plotting, displaying, and analyzing.

Because the charge amount inside the NG is fixed, achieving the maximum energy cycle requires the maximized NG voltage before the power releasing, which is related to the external load and discharge moment. Controlling discharge moment can be realized by a switch in series with the NG, as illustrated in Supplementary Fig. 8. With the modulation of switch, the voltage source in lumped circuit model of NG can be changed from sinusoid-wave source to square-wave source, and the photograph of *V-Q* curve acquisition system for these two different modes of ideal NG is shown in Fig. 5**c and** Supplementary Movie 2**.** By setting the external load as 1 GΩ, amplitude of voltage source as 20 V, and capacitance C_{in} as 100 pF, the encircled areas of the close loop in the *V-Q* curves from square-wave voltage source are significantly larger, indicating that the modulation of switch can help the TENG to output energy with the maximum energy cycle (MEC) (Fig. 5**d,** Supplementary Fig. 9).

We also compare the MEC measured by the ME and 6514 electrometer at an external load of 1GΩ. Benefiting from the improved voltage measurement accuracy, the area of MEC measured by the ME is much larger than that from the 6514 electrometer, and the measurement error of maximum energy output is reduced to 35.3%. If we can maximize the measurement accuracy until $V_m = V_{OC}$, the measured MEC would be further expanded to the region marked by the dashed line, as shown in Fig. 5**e**. When the TENG works at the MEC state**,** and the resistance is increased to 1 GΩ, the loop curve gradually gets close to the parallelogram of maximum loop curve (Fig. 5**f**). The influences of V_{OC} and C_{TENG} on the MEC are also presented in Supplementary Fig. 10. By measuring the *V-Q* curves of the simulated NG, the influences of the NG's output mode, internal parameters, and external load on the MEC are summarized.

Because the SFT mode TENG has a constant equivalent capacitance similar to the constructed ideal NG, it is chosen to systematically study the output cycles of a practical TENG (Fig. 5**g**). A switch is introduced to control the TENG to work at the maximum output state (Supplementary Fig. 11 **and** Supplementary Movie 3). With increasing the external load, the output cycles gradually approach the MEC at $R = 1$ GΩ (Fig. 5**h and** Supplementary Fig. 12). We notice that the measured transferred charge decreases slightly with the increase of *R*, because larger resistance causes more charges to flow through the voltmeter as illustrated in Fig. 5**g**. The MECs measured by the two instruments are compared as shown in Fig. 5**i**. Excessive instrument capacitance of 6514 electrometer not only reduces the measured voltage, but also leads to the loss of partial charges, which reduces the measured charge in the characterization process of MEC. Finally, the encircled area of *V-Q* curve measured by the 6514 electrometer is much lower than that of the theoretical MEC curve. Due to the improved measurement accuracy, the maximum energy output of the SFT-TENG in one cycle measured by the ME is improved to 1915.95 nW compared to the 540.72 nW from the 6514 electrometer.

3. Conclusions

In conclusion, the voltage measurement error caused by instrument internal capacitor is revealed and the strategy is proposed to improve the measurement accuracy of NGs in this work. In order to characterize this error and influencing factors, the influences of equivalent capacitance of NG and internal capacitance of instrument on the voltage measurement accuracy are systematically and quantitatively studied by constructing an ideal NG based on lumped model, and some experimental phenomena violating the theories are explained by this measurement error. For comparing the influence of electrometer capacitance on four working modes of TENGs, Multiphysics simulation models with the same charge amount are built to calculate their voltage variation at different capacitive loads to simulate the measurement process of the instrument. Based on that, the suitable internal capacitance of instrument is derived and a modified multi-functional electrometer is designed to evaluate the maximum output energy by measuring the *V-Q* cycle curves of TENG. Compared to commercial electrometer, the measured accuracy by the ME is significantly increased from 22.7% to 64.7%, and the maximum energy output of the SFT-TENG in one cycle is improved to 1915.95 nW compared to the 540.72 nW from the 6514 electrometer. In this paper, the analysis of existing problems in NGs characterization has important guiding meaning for the development of measurement technology and theoretical research of NGs. The provided measurement method and optimization strategy lay the foundation for building the standardized, and unified NG characterization system, which is more accurate, simple-accessible, and flexible. And the specially-designed hardware and software by our recently-established company (Naneng instrument technology Co., Ltd) can provide the measurement supports for the NG researches around the world.

4. Experimental section

4.1. Characterizations and measurements

The ideal nanogenerator is constructed by a capacitor and a voltage source. In the experiment, a data acquisition card (NI USB 6356) is used

as the voltage source to generate voltage signal with different waveforms with the maximum amplitude of ± 10 V, which can be controlled by the computer program based on LabVIEW. The commercial electrometer (Keithley 6514) is used to measure the transferred charge in the circuit during the characterization process, and the acquired data are transferred through a signal adapter (Naneng instrument technology Co., Ltd) to data acquisition program for recording and analyzing.

4.2. Finite element method simulation for four modes of TENG

The software of COMSOL MULTIPHYSICS is used to simulate the transient process of the TENG in multiple physical fields. The utilized physics in the model include electrostatic field, circuit and moving mesh. The length of electrode is set as 15.3 mm for four modes of TENGs and the surface charge density of dielectric layer is set as 1.17×10^{-5} C/m^2 in electrostatic field. Then the specified mesh displacement with the function of S/2[mm] + S/2[mm] * sin(2 * pi * t[1/s] + 3 * pi/2) is applied to the motion layer of TENG, and a capacitor is connected into the circuit by setting a terminal and ground node in the electrostatic field with the consistent label with the both endpoints of the capacitor. Besides the capacitor, other kinds of electronic component (such as resistor and inductor) can be added in the circuit using the same method to achieve different load simulations. After fully-coupled simulation, the voltage variation on external load with the motion of TENG can be calculated.

4.3. Fabrication of the modified multi-functional electrometer

The modified multi-functional electrometer is composed of 8 electrometer modules, an analog-to-digital converter (ADC), a spartan 6 FPGA chip, and a gigabit ethernet switch chip. Each electrometer module can be configured into voltmeter, coulombmeter, and ammeter for transferring the high voltage, transferred charge, and current signal into ± 5 V voltage signal. Then, this analog voltage signal will be transferred into digital signal by ADC and sent to a computer through the ethernet chip after the processing of FPGA. When it is used to acquire *V-Q* cycle curves of NGs, two of eight channels of the modified electrometer are utilized, and they are configured into voltmeter and coulombmeter to measure the voltage on the resistor and transferred charge in the circuit, respectively (Supplementary Fig. 13).

CRediT authorship contribution statement

J.A. conceived the idea. **T.J.** and **Z.L.W.** conducted the work and supervised the experiments. **J.A.** and **T.J.** prepared the manuscript. **J.A.** and **P.C.** designed and performed the electrical measurements. **J.A.** designed the modified multi-functional electrometer and signal acquisition system. **C.L.** helped for the development of the experimental setups. **F.L.** provided assistance with the finite element simulation. All the authors discussed the results and commented on the manuscript.

Declaration of Competing Interest

The authors declare that they have no known competing financial interests or personal relationships that could have appeared to influence the work reported in this paper.

Acknowledgements

This work was supported by the National Key R & D Project from Minister of Science and Technology (2021YFA1201604), National Natural Science Foundation of China (Grant nos. 51702018, 51432005, and 51561145021), and sponsored by CAS-TWAS President's Fellowship for international students. We also thank Yidan Wang for the design of some schematic diagrams in this paper.

Appendix A. Supporting information

Supplementary data associated with this article can be found in the online version at doi:10.1016/j.nanoen.2021.106884.

References

[1] R. Haight, W. Haensch, D. Friedman, Science 353 (2016) 124–125.
[2] Z.L. Wang, Rep. Prog. Phys. 84 (2021).
[3] E. Hittinger, P. Jaramillo, Science 364 (2019) 326–328.
[4] S. Park, S.W. Heo, W. Lee, D. Inoue, Z. Jiang, K. Yu, H. Jinno, D. Hashizume, M. Sekino, T. Yokota, K. Fukuda, K. Tajima, T. Someya, Nature 561 (2018) 516–521.
[5] J. An, P. Chen, Z. Wang, A. Berbille, H. Pang, Y. Jiang, T. Jiang, Z.L. Wang, Adv. Mater. 33 (2021) 2101891.
[6] J. An, Z. Wang, T. Jiang, P. Chen, X. Liang, J. Shao, J. Nie, M. Xu, Z.L. Wang, Mater. Today 41 (2020) 10–20.
[7] J. Chen, Y. Huang, N. Zhang, H. Zou, R. Liu, C. Tao, X. Fan, Z.L. Wang, Nat. Energy 1 (2016) 1–8.
[8] H. Guo, X. Pu, J. Chen, Y. Meng, M.-H. Yeh, G. Liu, Q. Tang, B. Chen, D. Liu, S. Qi, C. Wu, C. Hu, J. Wang, Z.L. Wang, Sci. Robot. 3 (2018) eaat2516.
[9] W. Gong, C. Hou, J. Zhou, Y. Guo, W. Zhang, Y. Li, Q. Zhang, H. Wang, Nat. Commun. 10 (2019) 868.
[10] S. Niu, X. Wang, F. Yi, Y.S. Zhou, Z.L. Wang, Nat. Commun. 6 (2015) 8975.
[11] F.-R. Fan, Z.-Q. Tian, Z. Lin Wang, Nano Energy 1 (2012) 328–334.
[12] Z.L. Wang, Science 312 (2006) 242–246.
[13] L. Wang, S. Liu, G. Gao, Y. Pang, X. Yin, X. Feng, L. Zhu, Y. Bai, L. Chen, T. Xiao, X. Wang, Y. Qin, Z.L. Wang, ACS Nano 12 (2018) 4903–4908.
[14] J.-H. Lee, K.Y. Lee, M.K. Gupta, T.Y. Kim, D.-Y. Lee, J. Oh, C. Ryu, W.J. Yoo, C.-Y. Kang, S.-J. Yoon, J.-B. Yoo, S.-W. Kim, Adv. Mater. 26 (2014) 765–769.
[15] L. Wang, S. Liu, X. Feng, C. Zhang, L. Zhu, J. Zhai, Y. Qin, Z.L. Wang, Nat. Nanotechnol. 15 (2020) 661–667.
[16] H. Wu, S. Wang, Z. Wang, Y. Zi, Nat. Commun. 12 (2021).
[17] Z. Wang, W. Liu, W. He, H. Guo, L. Long, Y. Xi, X. Wang, A. Liu, C. Hu, Joule 5 (2021) 441–455.
[18] R. Lei, Y. Shi, Y. Ding, J. Nie, S. Li, F. Wang, H. Zhai, X. Chen, Z.L. Wang, Energy Environ. Sci. 13 (2020) 2178–2190.
[19] Z.L. Wang, J. Chen, L. Lin, Energy Environ. Sci. 8 (2015) 2250–2282.
[20] F.B. Xi, Y.K. Pang, W. Li, T. Jiang, L.M. Zhang, T. Guo, G.X. Liu, C. Zhang, Z. L. Wang, Nano Energy 37 (2017) 168–176.
[21] L. Cheng, Q. Xu, Y. Zheng, X. Jia, Y. Qin, Nat. Commun. 9 (2018) 3773.
[22] W. Liu, Z. Wang, G. Wang, G. Liu, J. Chen, X. Pu, Y. Xi, X. Wang, H. Guo, C. Hu, Z. L. Wang, Nat. Commun. 10 (2019) 1426.
[23] J. Nie, Z. Wang, Z. Ren, S. Li, X. Chen, Z. Lin Wang, Nat. Commun. 10 (2019) 2264.
[24] H. Zhang, F. Marty, X. Xia, Y. Zi, T. Bourouina, D. Galayko, P. Basset, Nat. Commun. 11 (2020) 3221.
[25] A. Li, Y. Zi, H. Guo, Z.L. Wang, F.M. Fernandez, Nat. Nanotechnol. 12 (2017) 481–487.
[26] W.L. Liu, Z. Wang, G. Wang, Q.X. Zeng, W.C. He, L.Y. Liu, X. Wang, Y. Xi, H.Y. Guo, C.G. Hu, Z.L. Wang, Nat. Commun. 11 (2020) 1883.
[27] Z. Ren, Z. Wang, Z. Liu, L. Wang, H. Guo, L. Li, S. Li, X. Chen, W. Tang, Z.L. Wang, Adv. Energy Mater. 10 (2020) 2001770.
[28] J. Bae, J. Lee, S. Kim, J. Ha, B.S. Lee, Y. Park, C. Choong, J.B. Kim, Z.L. Wang, H. Y. Kim, J.J. Park, U.I. Chung, Nat. Commun. 5 (2014) 4929.
[29] H. Wang, L. Xu, Y. Bai, Z.L. Wang, Nat. Commun. 11 (2020) 1–9.
[30] J. An, Z.M. Wang, T. Jiang, X. Liang, Z.L. Wang, Adv. Funct. Mater. 29 (2019) 1904867.
[31] X. Liang, Z. Liu, Y. Feng, J. Han, L. Li, J. An, P. Chen, T. Jiang, Z.L. Wang, Nano Energy 83 (2021), 105836.
[32] X. Yang, L. Xu, P. Lin, W. Zhong, Y. Bai, J. Luo, J. Chen, Z.L. Wang, Nano Energy 60 (2019) 404–412.
[33] Z.L. Wang, Nature 524 (2017) 295.
[34] W. Xu, H. Zheng, Y. Liu, X. Zhou, C. Zhang, Y. Song, X. Deng, M. Leung, Z. Yang, R. X. Xu, Z.L. Wang, X.C. Zeng, Z. Wang, Nature 578 (2020) 392–396.
[35] J. Chen, Z.L. Wang, Joule 1 (2017) 480–521.
[36] Z. Wang, J. An, J. Nie, J. Luo, J. Shao, T. Jiang, B. Chen, W. Tang, Z.L. Wang, Adv. Mater. 32 (2020) 2001466.
[37] Y.C. Lai, J. Deng, R. Liu, Y.C. Hsiao, S.L. Zhang, W. Peng, H.M. Wu, X. Wang, Z. L. Wang, Adv. Mater. 30 (2018) 1801114.
[38] C. Chen, Z. Wen, J. Shi, X. Jian, P. Li, J.T.W. Yeow, X. Sun, Nat. Commun. 11 (2020) 4143.
[39] J. Jiang, Y. Zhang, Q. Shen, Q. Zhu, X. Ge, Y. Liu, Z. Wen, X. Sun, Nano Energy 89 (2021).
[40] Y. Zhang, M. Peng, Y. Liu, T. Zhang, Q. Zhu, H. Lei, S. Liu, Y. Tao, L. Li, Z. Wen, X. Sun, ACS Appl. Mater. Interfaces 12 (2020) 19384–19392.
[41] Z.L. Wang, Nano Energy 68 (2020), 104272.
[42] S. Niu, S. Wang, L. Lin, Y. Liu, Y.S. Zhou, Y. Hu, Z.L. Wang, Energy Environ. Sci. 6 (2013) 3576.
[43] S. Niu, Y.S. Zhou, S. Wang, Y. Liu, L. Lin, Y. Bando, Z.L. Wang, Nano Energy 8 (2014) 150–156.
[44] W. Zhang, G. Gu, H. Qin, S. Li, W. Shang, T. Wang, B. Zhang, P. Cui, J. Guo, F. Yang, G. Cheng, Z. Du, Nano Energy 77 (2020), 105108.

[45] W. Zhang, G. Gu, W. Shang, H. Luo, T. Wang, B. Zhang, P. Cui, J. Guo, F. Yang, G. Cheng, Z. Du, Nano Energy 86 (2021), 106056.
[46] J. Chen, J. Wang, W. Xuan, S. Dong, J. Luo, Sensors 20 (2020) 4838.
[47] Y. Zi, S. Niu, J. Wang, Z. Wen, W. Tang, Z.L. Wang, Nat. Commun. 6 (2015) 8376.

Jie An received his B.S. degree in Maritime Engineering from Dalian Maritime University in 2017. Now he is pursuing his Ph. D. degree in Beijing Institute of Nanoenergy and Nanosystems, Chinese Academy of Sciences. His research interests are mainly focused on clean energy harvesting and self-powered sensor systems based on triboelectric nanogenerator.

Pengfei Chen received his bachelor's degree at Dalian Maritime University in 2018. Now he is a doctoral candidate in Beijing Institute of Nanoenergy and Nanosystem, Chinese Academy of Science. His research interests are focused on blue energy harvesting and self-powered sensing.

Chengyu Li received his master degree from Guangxi University in 2021. Now he is currently pursuing his Ph.D. degree in Beijing Institute of Nanoenergy and Nanosystems, Chinese Academy of Sciences. His research interests are focused on micro/nano-devices, wearable/flexible electronics, and principle investigation of triboelectric nanogenerators.

Fangming Li is currently pursuing his Ph.D. degree in Dalian Maritime University, China. His research mainly focuses on triboelectric nanogenerators for high voltage applications.

Tao Jiang is a professor in the Beijing Institute of Nanoenergy and Nanosystems, Chinese Academy of Sciences. He received his B.S. and Ph.D. degrees from School of Materials Science and Engineering, in 2008 and 2014, respectively, from East China University of Science and Technology. After graduation, he worked in the Beijing Institute of Nanoenergy and Nanosystems as a postdoctoral research fellow. His research interests are the theoretical studies of triboelectric nanogenerators, and practical applications in blue energy harvesting.

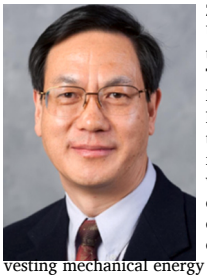

Zhong Lin Wang received his Ph.D. degree from Arizona State University in physics. He now is the Hightower Chair in Materials Science and Engineering, Regents' Professor at Georgia Tech, the chief scientist and director of the Beijing Institute of Nanoenergy and Nanosystems, Chinese Academy of Sciences. Prof. Wang has made original and innovative contributions to the synthesis, discovery, characterization and understanding of fundamental physical properties of oxide nanobelts and nanowires, as well as applications of nanowires in energy sciences, electronics, optoelectronics and biological science. His discovery and breakthroughs in developing nanogenerators establish the principle and technological road map for harvesting mechanical energy from environmental and biological systems for powering personal electronics. His research on self-powered nanosystems has inspired the worldwide efforts in academia and industry for studying energy for micro-nano-systems, which is now a distinct disciplinary in energy research and future sensor networks. He coined and pioneered the fields of piezotronics and piezophototronics by introducing piezoelectric potential gated charge transport process in fabricating new electronic and optoelectronic devices.